Neuron, Vol. 42, 789–801, June 10, 2004, Copyright ©2004 by Cell Press

Precise Development of Functional and Anatomical Columns in the Neocortex

Ingrid Bureau, Gordon M.G. Shepherd, and Karel Svoboda*
Howard Hughes Medical Institute
Cold Spring Harbor Laboratory
Cold Spring Harbor, New York 11724

Summary

Sensory cortex is ordered into columns, each tuned to a subset of peripheral stimuli. To identify the principles underlying the construction of columnar architecture, we monitored the development of circuits in the rat barrel cortex, using laser-scanning photostimulation analysis of synaptic connectivity, reconstructions of axonal arbors, and in vivo whole-cell recording. Circuits impinging onto layer 2/3 neurons from layers 4 and 2/3 developed in a monotonic, precise progression, with little evidence for transient hyperinnervation at the level of cortical columns. Consistent with this, synaptic currents measured in layer 2/3 neurons at PND 8, just after these neurons ceased to migrate, revealed already spatially well-tuned receptive fields.

Introduction

Sensory cortices contain arrays of cortical columns arranged into topographic maps (Hubel and Wiesel, 1962; Mountcastle, 1957), wherein neurons in one cortical column receive input from a particular region of sensory space. Cortical mechanisms of sensory processing rely on highly organized intracortical synaptic circuits. What events lead to the organization of these circuits? The dominant model involves a transient state of diffuse connectivity, followed by a process of refinement through pruning (Katz and Shatz, 1996). This mechanism operates at the neuromuscular junction (Lichtman and Colman, 2000) and the retinogeniculate (Campbell and Shatz, 1992; Chen and Regehr, 2000) and retinocollicular (Brown et al., 2000) maps. The involvement of pruning in the establishment of the thalamocortical projection (Crowley and Katz, 2002) and the odor map in the olfactory bulb (Lin et al., 2000; Zheng et al., 2000) is controversial. Intracortical laminar targeting develops with considerable specificity (Callaway and Lieber, 1996; Katz, 1991; but see Borrell and Callaway, 2002).

To identify mechanisms underlying the development of cortical circuits, we examined the construction of intracortical circuitry defining columns in the barrel cortex. Thalamocortical inputs carrying excitation from individual whiskers are anatomically segregated in layer 4 into barrels (Bernardo and Woolsey, 1987; Killackey and Leshin, 1975; White and DeAmicis, 1977). Barrels form soon after birth (Agmon et al., 1993; Jhaveri et al., 1991; Killackey et al., 1995; Schlaggar and O'Leary, 1994) and can be visualized in living (Agmon and Connors, 1991; Finnerty et al., 1999) and fixed (Woolsey and Van der Loos, 1970) slices. After the first postnatal week, barrels become insensitive to manipulations at the periphery, such as lesions of the whisker follicles (Rice and Van der Loos, 1977; Schlaggar et al., 1993; Van der Loos and Woolsey, 1973; Waite and Taylor, 1978). The anatomical barrel map can then be used as a stable picture of the normal columnar organization, against which developmental changes of synaptic circuitry and receptive field structure can be measured with great sensitivity (Fox, 1992).

Between the layer 4 barrels are the septa, which are associated with distinct thalamocortical (Chmielowska et al., 1989; Kim and Ebner, 1999; Koralek et al., 1988; Lu and Lin, 1992) and intracortical (Kim and Ebner, 1999; Shepherd et al., 2003) circuits. Barrels and septa can be used to define barrel- and septum-related columns spanning the vertical extent of cortex (Figure 1A). Neurons in one barrel-related column are excited best by a particular (principal) whisker and less by surrounding whiskers (Armstrong-James and Fox, 1987; Simons, 1978), while neurons in septum-related columns have broad receptive fields (Brecht et al., 2003; Brecht and Sakmann, 2002).

Layer 2/3 pyramidal cells migrate into place until PND 6 (Ignacio et al., 1995). During the second postnatal week, cortical circuits develop rapidly. Layer 2/3 dendritic arbors elaborate (Maravall et al., 2004a), as do the axons projecting from layer 4 to layer 2/3 (Bender et al., 2003). Simultaneously, the density of cortical synapses (Micheva and Beaulieu, 1996) and the amplitude of whisker deflection-evoked postsynaptic potentials measured in layer 2/3 neurons in vivo increase several-fold (Stern et al., 2001). At the end of the second postnatal week, layer 2/3 receptive fields have mature structure (Brecht et al., 2003; Stern et al., 2001; Zhu and Connors, 1999). Within barrel-related columns, excitatory axons from layer 4 to layer 2/3 form a precise feedforward circuit, projecting almost exclusively within a single barrel column (Bender et al., 2003; Brecht and Sakmann, 2002; Lubke et al., 2003; Petersen and Sakmann, 2001). This is reflected in the distributions of synaptic inputs to layer 2/3, which also obey strict columnar boundaries (Shepherd et al., 2003). In septum-related columns, layer 2/3 cells are weakly coupled to presynaptic layer 4 neurons (Shepherd et al., 2003).

How does this columnar circuitry develop? To address this question, we combined an analysis of functional connectivity in brain slices using laser-scanning photostimulation (LSPS) (Callaway and Katz, 1993; Dalva and Katz, 1994; Roerig and Kao, 1999; Schubert et al., 2001) with morphological analysis of axonal arbors (Bender et al., 2003; Brecht and Sakmann, 2002; Lubke et al., 2003; Petersen and Sakmann, 2001). We describe the progressive divergence of circuits related to barrels and to septa (Brecht et al., 2003; Brecht and Sakmann, 2002; Kim and Ebner, 1999; Shepherd et al., 2003). We find that layer 4 → 2/3 circuits develop with great specificity and without detectable pruning at the level of cortical columns. Consistent with these findings, even the earliest

*Correspondence: svoboda@cshl.org

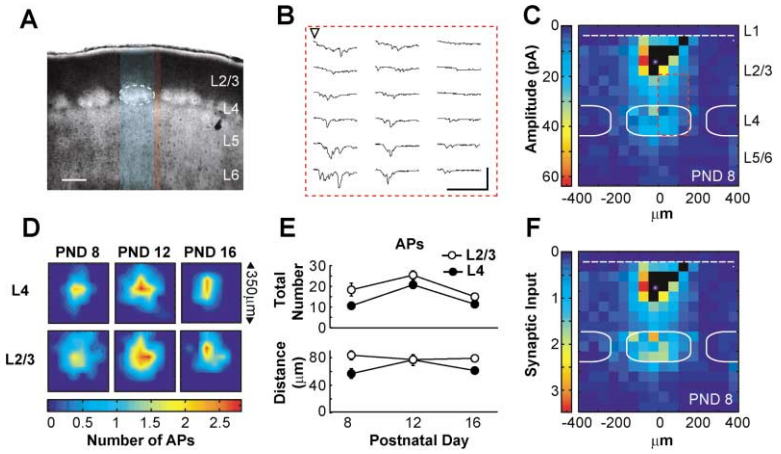

Figure 1. Laser-Scanning Photostimulation Mapping of Intracortical Synaptic Circuits

(A) Brain slice of rat somatosensory cortex at PND 8, showing barrels and septa under bright-field illumination. One of the barrels is demarcated by a dashed white line. Its barrel-related column is shown in blue. Between the barrels in layer 4 are septa; one of the septum-related columns is shown in red. Scale bar equals 300 μm.

(B) Examples of individual postsynaptic responses recorded from a layer 2/3 pyramidal neuron during LSPS mapping of synaptic inputs in layer 2/3 and 4. Glutamate was uncaged at an array of sites corresponding to the red box in (C). Arrowhead indicates the timing of the 1 ms UV stimulus. Scale bars equal 100 ms and 100 pA.

(C) Map of synaptic responses (average of two individual maps). Colors represent the mean amplitude of synaptic current measured in a window of 7 to 100 ms after photostimulation. Photostimuli were delivered every 1.5 s. Black squares indicate pixels where the large amplitudes of direct responses, due to overlap of the uncaging spot with dendrites of the recorded neuron, precluded accurate estimation of synaptic responses. Dashed white line indicates the border between layers 1 and 2. Solid white lines indicate barrel boundaries. Dashed red box indicates the area corresponding to the sample traces in (B).

(D) Excitation profiles of layer 4 neurons (upper row) and layer 2/3 neurons (lower row) recorded at three ages. Colors represent the mean number of action potentials (APs) recorded in loose-patch mode in a 100 ms window after photostimulation. The grid was centered on the somata.

(E) Development of excitation profiles. Upper, the total number of APs evoked per cell as a function of developmental age. Lower, mean distance from the soma at which APs were evoked, calculated as Σ(Aps $\times$ distance from soma)/Σ(APs).

(F) Synaptic input maps. The map in (C) was normalized to the total number of APs per layer.

layer 2/3 receptive fields measured in vivo are highly tuned.

Results

Mapping the Development of Intracortical Circuits with LSPS

We mapped the development of excitatory inputs to layer 2/3 pyramidal neurons at three developmental ages. (1) At PND 8, layer 2/3 pyramidal cells have migrated into place (Ignacio et al., 1995) and begin to sprout processes (Callaway and Katz, 1990; Maravall et al., 2004a). (2) At PND 12, layer 2/3 pyramidal cells have largely mature dendritic morphology (Maravall et al., 2004a) but are only weakly driven by sensory stimulation (Stern et al., 2001). (3) At PND 16, layer 2/3 pyramidal cells have mature receptive fields (Stern et al., 2001). This range of developmental ages also coincides with a 5-fold increase in synaptic density (Micheva and Beaulieu, 1996). In slices cut orthogonal to barrel rows, barrels and septa can be readily visualized (Figure 1A; Finnerty et al., 1999; Shepherd et al., 2003; Welker and Woolsey, 1974). We recorded from neurons in layers 2 and 3 above barrels and septa and mapped the distributions of excitatory neurons presynaptic to the recorded neuron using LSPS (Shepherd et al., 2003). Glutamate was photoreleased in the focal spot of a UV laser beam on a 16 $\times$ 16 pixel grid. Postsynaptic responses were measured as the average current during a 100 ms response window (Figure 1B; Experimental Procedures). At a particular spot (i.e., pixel) on the grid (Figure 1C), the amplitude of the postsynaptic response was then proportional to the number of neurons stimulated (N_{cell}), the number of action potentials (APs) fired per stimulated neuron (N_{AP}), and the average strength of the synaptic connection with the stimulated presynaptic neuron (I_{con}): pixel value $\propto N_{cell}$ N_{AP} I_{con}.

The number of APs evoked in neurons by glutamate uncaging ("excitability") depends on multiple factors, including the density of glutamate receptors, the capacity of glutamate clearance systems, the input impedance of neurons, the properties of voltage-gated conductances, etc. Many of these factors are known to undergo profound developmental changes (Brennan et al., 1997; Maravall et al., 2004b; Ullensvang et al., 1997; Zhu, 2000). Therefore, to probe selectively the development of synaptic inputs, we corrected for developmental changes in excitability by measuring over development the number of APs triggered by glutamate uncaging (Figure 1D; Shepherd et al., 2003). Under our experimental conditions, APs were triggered only when the UV spot was near the soma (60–80 μm away on average; Figure 1D). Furthermore, the excited neurons did not cause spiking in other neurons (Shepherd et al., 2003). The mean distance from sites of photoexcitability to the soma (a parameter that estimates the spatial resolution for stimulating presynaptic neurons) did not vary significantly with developmental age (Figure 1E), indicating that our ability to resolve subcolumnar and sublaminar organization of neuronal connectivity was similar across all ages. The total number of APs evoked by identical stimuli increased between PND 8 and PND 12 and decreased again by PND 16 (Figure 1E). At each developmental time point, the mean total number of APs evoked was used to scale the input maps layer-wise for laminar differences in presynaptic excitability (Figure 1F). Over the developmental ages tested, changes in neuronal density are modest. Developmental differences in the scaled maps can then be interpreted in terms of differences in synaptic connectivity; pixel values are proportional to

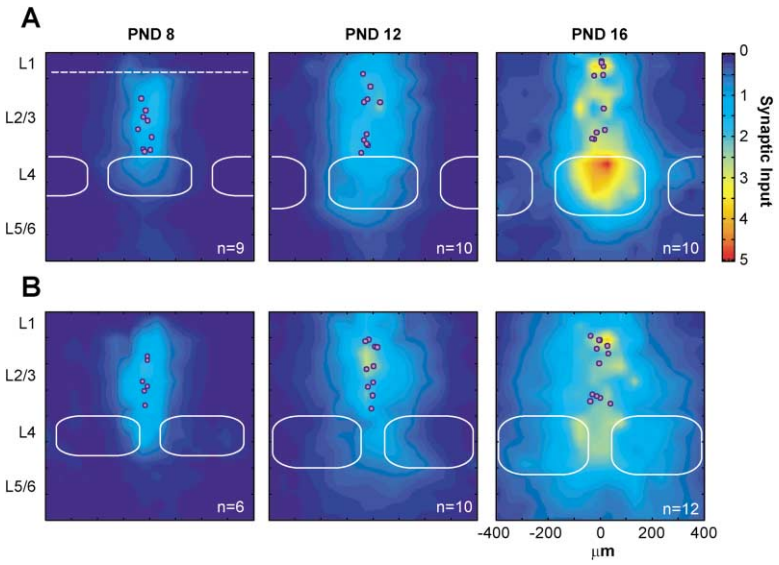

Figure 2. Development of Synaptic Input Maps for Layer 2/3 Pyramidal Neurons

Left, PND 8; middle, PND 12; right, PND 16. White shapes indicate the barrels used for alignment. Purple circles indicate the positions of individual somata.

(A) Neurons above barrels.

(B) Neurons above septa.

the number of excitatory synaptic connections and their strength, termed here "synaptic input": pixel value (synaptic input) $\propto I_{con}$.

Layer 4 of barrel cortex is parceled anatomically and functionally into barrels and septa (Woolsey and Van der Loos, 1970). This segmentation is projected onto layer 2/3 neurons above barrels and septa, with cells above septa receiving less input originating from layer 4 on average than cells above barrels (Shepherd et al., 2003). We therefore separated our analysis into two groups: "barrel-related" and "septum-related" layer 2/3 cells (Figures 1A and 2). Since there was high variability for maps recorded from different cells, we averaged across cells in a group, using barrels and septa for alignment. At PND 8 both groups of cells received most of their input from nearby layer 2/3 cells, with little input from layer 4. With increasing age, both groups gained synaptic input from layer 2/3 as well as from layer 4. However, inputs from layer 4 increased less rapidly for neurons above septa than for those above barrels, resulting in the weak coupling between layer 4 and septum-related neurons (Shepherd et al., 2003). To gain insight into possible mechanisms of circuit development, we analyzed the emergence of synaptic input to layer 2/3 neurons from granular and supragranular sources in more detail.

Development of Layer 4 → 2/3 Circuits

Neurons above barrels rapidly gained excitatory synaptic input from layer 4 with development (factor of 2.0 between PND 8 and 12; 3.3 between PND 12 and 16; see Experimental Procedures). We measured the spatial distributions of input from layer 4 by averaging synaptic input maps across layer 4 (Figure 3A). At all ages, layer 4 inputs had high spatial acuity: synaptic input was highest immediately below the recorded neuron and decreased rapidly with horizontal distance (Figure 3B). This spatial tuning did not change with age, since inputs increased in the same proportion in and out of the barrel-related column (Figure 3C). As a result, the mean horizontal distance of synaptic inputs was constant during development and well within the width of a barrel (Figure 3D).

Neurons above septa also gained input from layer 4 with development, but less rapidly than neurons above barrels (factor of 1.3 between PND 8 and 12; 2.8 between PND 12 and 16; Figure 3E). As a result, layer 2/3 neurons above septa received less input originating from layer 4 than did cells above barrels (Shepherd et al., 2003). These barrel/septum differences were maintained in mature circuits (PND $\sim$30), where barrel-related cells received about double the synaptic input from layer 4 compared to septum-related cells (data not shown). The spatial distribution of input from layer 4 was narrow at the earliest ages and broadened with development: inputs horizontally farther from the recorded neuron increased more rapidly than inputs directly below (Figure 3F) (normalized spatial distributions at PND 8 and 16 are significantly different, Wilcoxon, $p < 0.05$). This is reflected in an upward trend in the mean horizontal distance of input with development, and at PND 16, cells above septa received inputs from significantly more distant layer 4 presynaptic cells than did cells above barrels (Mann-Whitney, $p < 0.01$; Figure 3D). These measurements revealed that the spatial distribution of excitatory input from layer 4 to layer 2/3 neurons did not sharpen with development. Instead, neurons above septa gained inputs from distant regions.

Development of Layer 2/3 Local Connections

A similar analysis was applied to the development of horizontal connections in layer 2/3. Neurons above barrels gained excitatory input from other layer 2/3 neurons mostly between PND 8 and 12 (factor of 2.2 between PND 8 and 12; 1.5 between PND 12 and 16). We measured the spatial distributions of synaptic input from layer 2/3 by averaging synaptic input maps across layer 2/3 (Figure 4A). We omitted a thin (100 μm) vertical band from the analysis because strong direct responses made quantitative recovery of synaptic responses difficult. At the youngest ages tested, layer 2/3 inputs were highly localized: synaptic inputs decreased rapidly with hori-

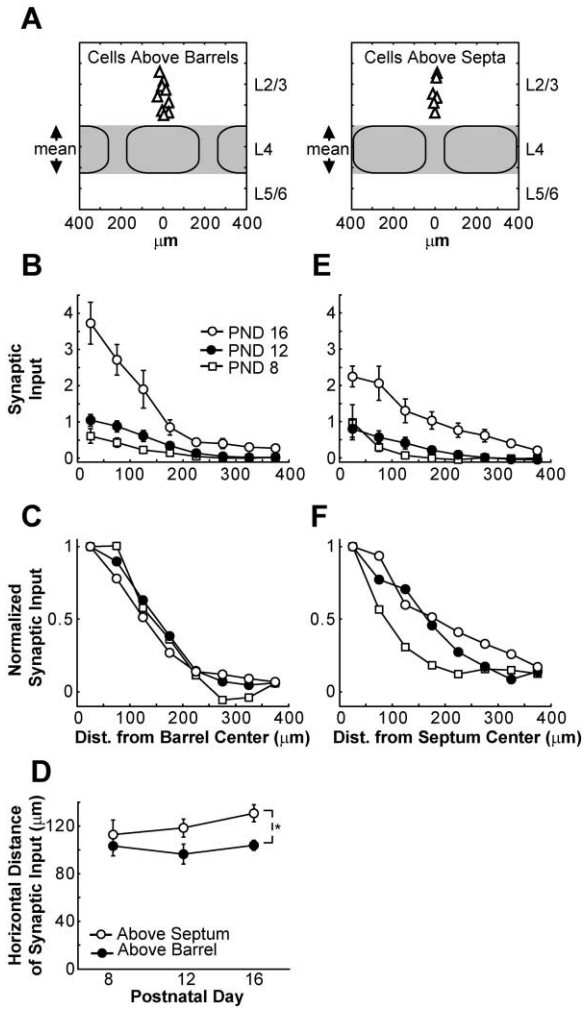

Figure 3. Horizontal Profile of Interlaminar Connectivity: Development of Synaptic Input from Layer 4 to Layer 2/3

(A) Schematics of the analysis. Synaptic input was averaged vertically across layer 4 (gray band) and analyzed separately for barrel-related (left) and septum-related (right) neurons.

(B) Spatial distributions of synaptic input from layer 4 for barrel-related layer 2/3 cells. Position zero corresponds to the center of the barrel. Data from positions on both sides of zero were combined to generate a single average distribution.

(C) Same data as in (B), normalized to the initial amplitude.

(D) The mean distance of layer 4 synaptic inputs to layer 2/3 cells, calculated as Σ(synaptic input $\times$ horizontal distance from soma)/Σ(synaptic input). Asterisk indicates a significant difference (Mann-Whitney, $p < 0.001$).

(E) Spatial distributions of synaptic input from layer 4 for septum-related layer 2/3 cells.

(F) Same data as in (E), normalized.

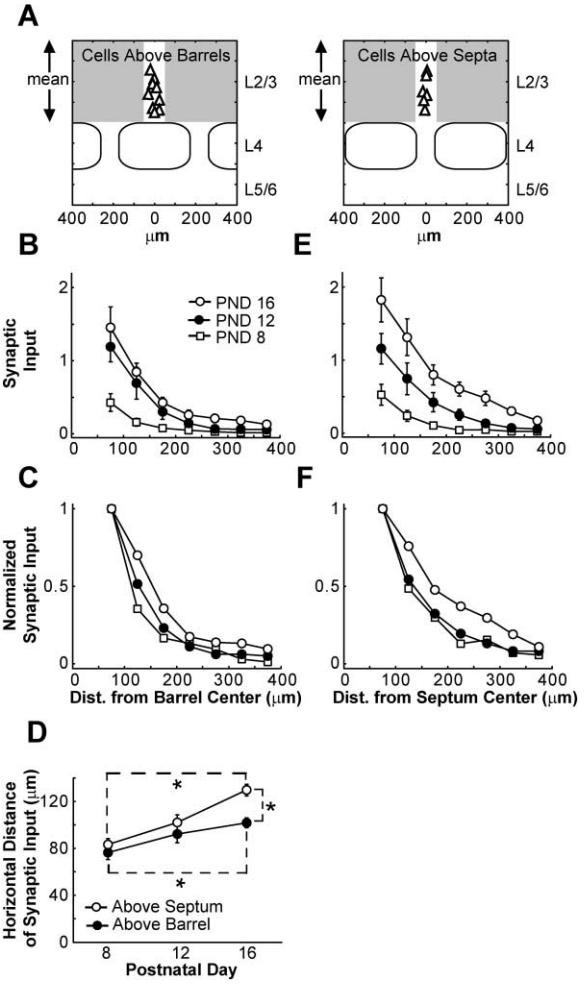

Figure 4. Horizontal Profile of Intralaminar Connectivity: Development of Synaptic Input from Layer 2/3 to Layer 2/3

(A) Schematics of analysis. Synaptic input was averaged vertically across layer 2/3 (gray band). A thin band around the somata (vertical white band) was omitted because strong direct responses precluded reliable estimates of synaptic inputs.

(B) Spatial distributions of synaptic input from layer 2/3 for barrel-related layer 2/3 cells.

(C) Same data as in (B), normalized.

(D) The mean distance of layer 2/3 synaptic inputs to layer 2/3 cells, calculated as Σ(synaptic input $\times$ horizontal distance from soma)/Σ(synaptic input). Asterisks indicate significant differences (Mann-Whitney, $p < 0.005$).

(E) Spatial distributions of synaptic input from layer 2/3 for septum-related layer 2/3 cells.

(F) Same data as in (E), normalized.

zontal distance (Figure 4B). With developmental age, layer 2/3 neurons connected with increasingly distant layer 2/3 neurons (Figure 4C). As a result, the mean horizontal distance of inputs increased with development (Figure 4D; Mann-Whitney, $p < 0.001$).

Neurons above septa continuously gained excitatory input from other layer 2/3 neurons with developmental age (factor of 2.0 between PND 8 and 12; 1.4 between PND 12 and 16; Figure 4E). Like barrel-related cells, they connected with increasingly more distant layer 2/3 neurons (Mann-Whitney, $p < 0.001$; Figures 4D and 4F). However, at PND 16, cells above septa received inputs from significantly more distant presynaptic cells than did cells above barrels (Mann-Whitney, $p < 0.005$; Figure 4D). Thus, our analysis reveals that the spatial distribution of excitatory synaptic input from layer 2/3 to layer 2/3 neurons is initially very local and broadens with development as neurons selectively gain input from more distant regions.

Differences in Synaptic Input Maps for Layer 2 and Layer 3 Neurons

The layer 2/3 synaptic input maps described here are similar to the maps reported in a previous study from

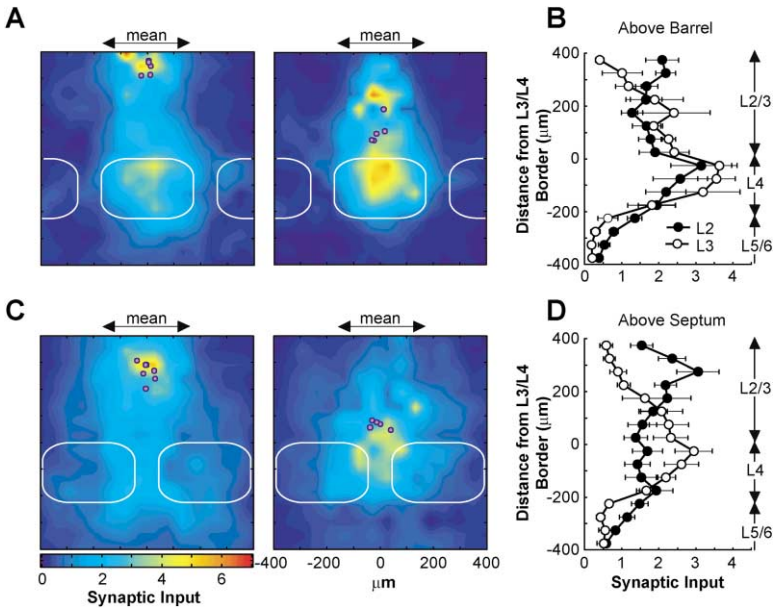

Figure 5. Vertical Profile of Intralaminar Connectivity: Differences in Synaptic Connectivity for Layer 2 and Layer 3 Pyramidal Cells

(A) Synaptic input maps for superficial (layer 2; right panel) and deep (layer 3, left panel) barrel-related pyramidal cells (PND 16).

(B) Distribution of synaptic inputs to superficial (layer 2, black circles) and deep (layer 3, open circles) cells as a function of vertical distance. The input was averaged horizontally across a band indicated by arrows in (A).

(C) Same as (A) for septum-related cells.

(D) Same as (B) for septum-related cells.

our laboratory. However, we noted some quantitative differences with respect to barrel/septum organization: septum-related cells received comparable input from layer 2/3 and layer 4, whereas our previous results found much weaker coupling with layer 4 compared to layer 2/3 (Shepherd et al., 2003). One key difference is that previously we had restricted ourselves to recording from superficial neurons, ~200 μm from the layer 3/4 border (Shepherd et al., 2003). To examine the possibility that laminar differences between layer 2 and layer 3 could account for the observed discrepancy, we separately analyzed deep cells (layer 3, <200 μm from the layer 3/4 border) and superficial cells (layer 2, >200 μm from the layer 3/4 border) (Figures 5A and 5C). Synaptic input maps for layer 2 and layer 3 cells differed. In general, layer 3 cells received stronger input from layer 4 than layer 2 cells (Figures 5B and 5D). This difference was especially pronounced in septum-related columns, for which layer 2 cells were only weakly coupled to layer 4, consistent with our previous report (differences between septum-related layer 2 and layer 3 cells, $p < 0.01$, KS test).

Layer 2 and layer 3 pyramidal cells differed further with respect to the structure of the input from layer 2/3. Layer 2 cells received stronger input from layer 3 than layer 3 cells from layer 2 (Figures 5B and 5D). Thus, deeper cells tend to relay information from layer 4 to more superficial cells, with little direct feedback. The differences between layer 2 and layer 3 were more pronounced in septum-related columns, where layer 2 neurons received input primarily from other layer 2/3 cells rather than layer 4 cells. Therefore, layer 2 septum-related neurons appear to function as higher-order relays compared to layer 3 septum-related neurons or barrel-related neurons, which are more strongly driven by layer 4.

Development of Layer 4 Axons

Our analysis of intracortical circuits impinging onto layer 2/3 neurons suggests that these circuits grow monotonically, with little evidence for transient developmental hyperconnectivity (Figure 2). However, our analysis using LSPS is only sensitive to functional circuits. This leaves open the possibility that axonal projections are transiently overarborized, without functional synaptic circuits, and then refined with developmental age (Katz and Shatz, 1996). We compared the development of synaptic input from layer 4 to layer 2/3 with the development of axonal projections ascending from layer 4 to layer 2/3 (Bender et al., 2003; Brecht and Sakmann, 2002; Lubke et al., 2003; Petersen and Sakmann, 2001). Individual layer 4 cells in brain slices were filled with biocytin (Figure 6A). Axonal arbors were reconstructed in three dimensions, and the density of axonal length (Brecht and Sakmann, 2002) was measured on a grid that matched synaptic input maps (Figures 6B and 6C; see Experimental Procedures).

For layer 4 cells in barrels, the axonal density projecting to layer 2/3 increased rapidly with development (factor of 2.0 between PND 8 and 12; 1.9 between PND 12 and 16; Figure 7A). We measured the horizontal spread of axonal branching (Figure 7B). Normalized plots of axonal density revealed that the spread of axons across rows in layer 2/3 was similar at all developmental ages (Figure 7C). Thus, similar to the distributions of functional synaptic input from layer 4 impinging onto layer 2/3 cells, layer 4 axons grow into layer 2/3 in a monotonic fashion, predominantly respecting barrel boundaries. We found little evidence for loss of axonal projections, consistent with previous studies (Bender et al., 2003).

For layer 4 septum cells, the rate of axonal growth into layer 2/3 was lower than for barrel cells (factor of 1.5 between PND 8 and 12; 1.8 between PND 12 and 16; Figures 7D and 7E). Septum cell axons initially grew in a narrow column in layer 2/3, similar to barrel cell axons (Figures 6B and 6C). However, after PND 12 they elaborated substantially into both neighboring barrels (Figures 6C, 7E, and 7F), and the half-width of horizontal distribution of axonal projections exceeded the half-width of septa at PND 16 (t test, $p < 0.001$).

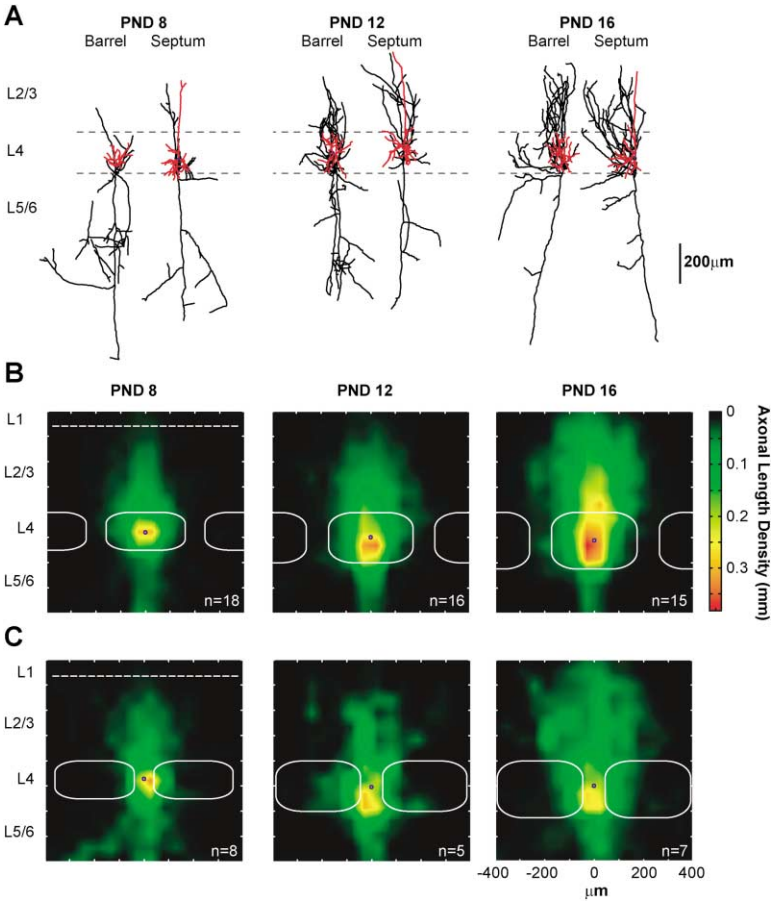

Figure 6. Development of Layer 4 Axons Projecting to Layer 2/3

(A) Examples of the morphology of excitatory neurons in layer 4 (dendrites, red; axons, black). Dashed lines indicate the borders of layer 4.

(B) Distributions of axonal length density for layer 4 barrel neurons. For averaging, individual cells were aligned on their somata. Colors represent the total length of axon segments calculated per 50 × 50 × (slice thickness) voxel averaged across cells. White shapes indicate the barrels and the dashed lines the border between layers 1 and 2.

(C) Same as (B) for layer 4 septum neurons.

A direct comparison revealed that the growth rates of axonal density and synaptic inputs originating from layer 4 were similar (Figure 7H). However, cell density in layer 4 decreases during development due to a concomitant increase in cortical volume (~30%–40%, data not shown). Therefore, our synaptic input maps underestimate the developmental increase in synaptic coupling between layers 4 and 2/3, and the growth of synaptic input per cell exceeds the rate of growth of axonal density. Rates of synapse formation and maturation (Lev et al., 2002; Takahashi et al., 2003) could contribute to this difference in time course.

Whole-Cell Recordings in the Developing Barrel Cortex In Vivo

Our in vitro experiments point to a precise process of circuit maturation without diffuse intermediates. These observations predict that receptive fields in layer 2/3 should be sharp even at early developmental stages. Since neurons in the developing cortex are rarely driven to threshold by sensory stimuli (Albus and Wolf, 1984; Armstrong-James, 1975; Fregnac and Imbert, 1978; Hubel and Wiesel, 1963), we used whole-cell voltage clamp measurements (Borg-Graham et al., 1998; Leinekugel et al., 2002) to measure maps of sensory-evoked excitatory postsynaptic currents (seEPSCs) in the developing (PND 8–18) barrel cortex. Recorded neurons ($n = 22$) were loaded with biocytin (Figure 8A). All recovered cell bodies (13/22) were in layer 2/3 and were spiny, and thus presumably excitatory. Whole-cell recording techniques have sufficient sensitivity to detect unitary currents in vivo (Figure 8B). At holding potentials of -70 mV, spontaneous currents had rapid kinetics (20%–80% rise time, 1.7 ± 0.1 ms; half decay time, 7.1 ± 0.6 ms), as expected for events dominated by AMPA-Rs.

In previous measurements, we could not reliably detect responses evoked by whisker stimulation at PND 12 or earlier (Stern et al., 2001). Local field potential measurements in layer 2/3 revealed that this may be in part due to the short interstimulus intervals (ISI = 3 s) used in these experiments, which produced synaptic depression in young (PND 8–11) but not in older (PND 16–17) animals (Figure 8C; Armstrong-James, 1975). With longer ISI (15 s), such depression was not seen in young animals, while potentiation was produced in older animals (Figure 8C). These developmental changes in short-term synaptic plasticity could be due to a decrease of synaptic fatigue (Armstrong-James, 1975; Stern et al., 2001) or to changes in the expression of presynaptic receptors (Kidd et al., 2002) with development.

With long ISIs, seEPSCs could be detected even at the youngest ages probed (PND 8). seEPSCs consisted of a barrage of synaptic events, often spread out over hundreds of milliseconds poststimulus (Figure 8D). We focused our analysis on the peak of the shortest latency synaptic events following deflection of the principal whisker (latencies to onset: PND 8–12, 32 ± 2 ms; PND

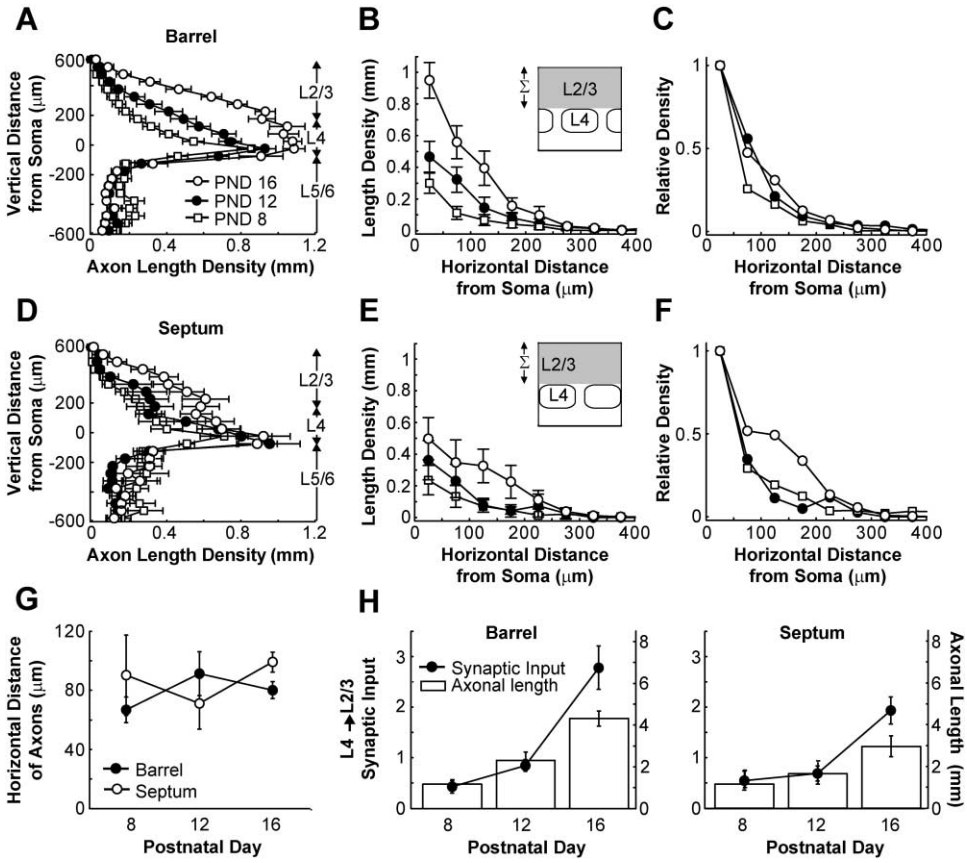

Figure 7. Analysis of the Development of Layer 4 Axons in Layer 2/3

(A) Axonal length density of barrel neurons as a function of vertical distance from their soma. Axonal length density was summed horizontally. Somata were aligned at zero. Note the large vertical expansion of axonal density into layer 2/3 with development.

(B) Horizontal distribution of layer 4 cell axonal length density in layer 2/3. Axonal length density was summed vertically across layer 2/3 (gray band in inset). Somatic positions were at zero along the *x* axis. Data were analyzed on both sides of zero and combined to generate a single average distribution.

(C) Same data as in (B), normalized.

(D–F) Septum cells, same analysis as in (A)–(C).

(G) Mean horizontal distance of layer 4 cell axons projecting into layer 2/3, calculated as Σ(axonal length density in layer 2/3 $\times$ horizontal distance from soma)/Σ(axonal length density in layer 2/3).

(H) Comparison of the development of layer 4 → 2/3 synaptic input and layer 4 → 2/3 axonal density. Plot of synaptic inputs originating from layer 4 (black circles) and of total axonal length in layer 2/3 (open bars) for barrel- (left) and septum- (right) related cells. Values are the averages across cells of pixel values in a window with a width of 250 μm and a height equal either to that of layer 4 (for synaptic inputs) or layers 1 through 3 (for the total axonal length).

15–18, 15 ± 1 ms; Figures 8D and 9B). These early responses likely reflect the most direct ascending excitation from layer 4 to layer 2/3 (Moore and Nelson, 1998; Zhu and Connors, 1999). Their amplitudes were small (range, 10–300 pA; average, 79 ± 16 pA), consistent with the firing of a single or few presynaptic neurons.

Development of Layer 2/3 Receptive Fields

To characterize receptive fields, we measured seEPSCs in response to deflections of multiple single whiskers in two age groups (PND 8–12, n = 15; PND 15–18, n = 7). Remarkably, even in the youngest animals probed, receptive fields were found to be mature, as judged by three criteria (Figure 9). First, in neurons that were recovered histologically, the whisker producing the largest response corresponded to the anatomically correct principal whisker (5/7; in two neurons they were nearest neighbors). Second, seEPSCs decreased in amplitude with distance from the principal whisker, similar to sensory evoked synaptic potentials measured in more mature animals (Figures 9A–9D; Brecht and Sakmann, 2002; Moore and Nelson, 1998; Stern et al., 2001; Zhu and Connors, 1999). seEPSCs evoked by the first surround whisker were smaller (~50%) than those evoked by the principal whisker (Figures 9C and 9D). Third, latencies increased with distance from the principal whisker (Figure 9E; Armstrong-James and Fox, 1987; Brecht and Sakmann, 2002; Moore and Nelson, 1998; Zhu and Connors, 1999).

In older rats (PND 15–18, n = 7), the amplitudes of seEPSCs were larger (1.6- to 1.8-fold; MANOVA, $p < 0.05$; Figure 9C) and the latencies of seEPSCs were shorter than at younger ages (Figure 9E) for all whiskers (Armstrong-James and Fox, 1987; Brecht and Sakmann,

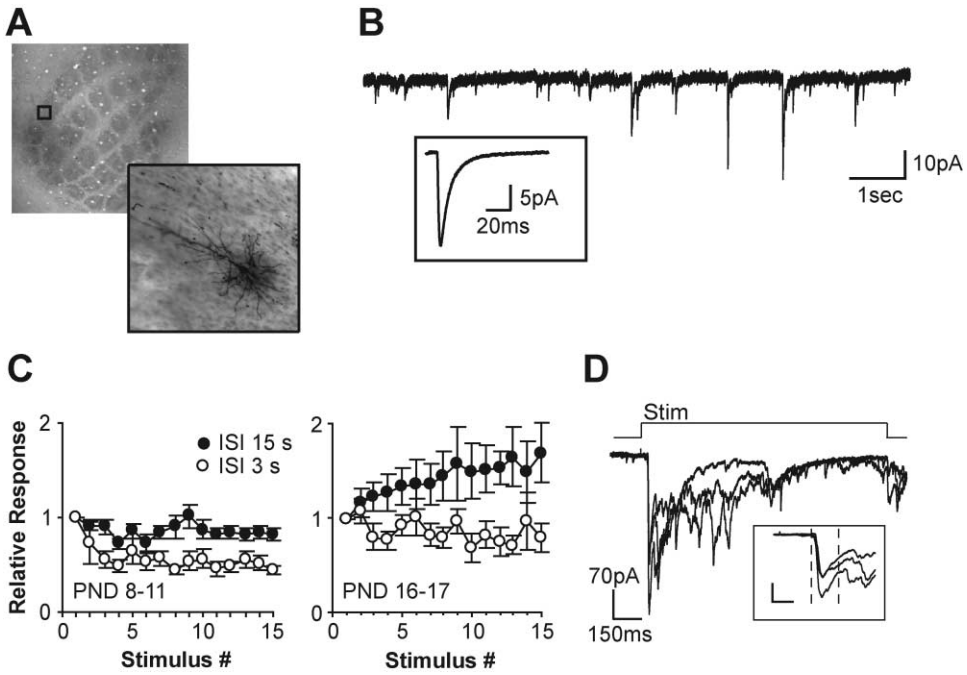

Figure 8. In Vivo Whole-Cell Recordings of Synaptic Currents in Developing Layer 2/3 Pyramidal Cells

(A) Layer 2/3 pyramidal cell labeled with biocytin (right) and its location with respect to the barrel map (box, left).

(B) Spontaneous synaptic currents. Inset, average of spontaneous synaptic currents.

(C) Relative amplitude of local field potentials as a function of stimulus number (open circle, ISI = 3 s; closed circle, ISI = 15 s) in PND 9–11 rats (left) and PND 15–17 rats (right).

(D) Whisker-evoked excitatory postsynaptic currents (seEPSCs). Three consecutive trials are shown. Inset, the same traces at an expanded scale (scale bars, 20 ms and 100 pA). The peak amplitude of the early response was measured within a time window (dashed lines) set to measure ascending input from layer 4 only.

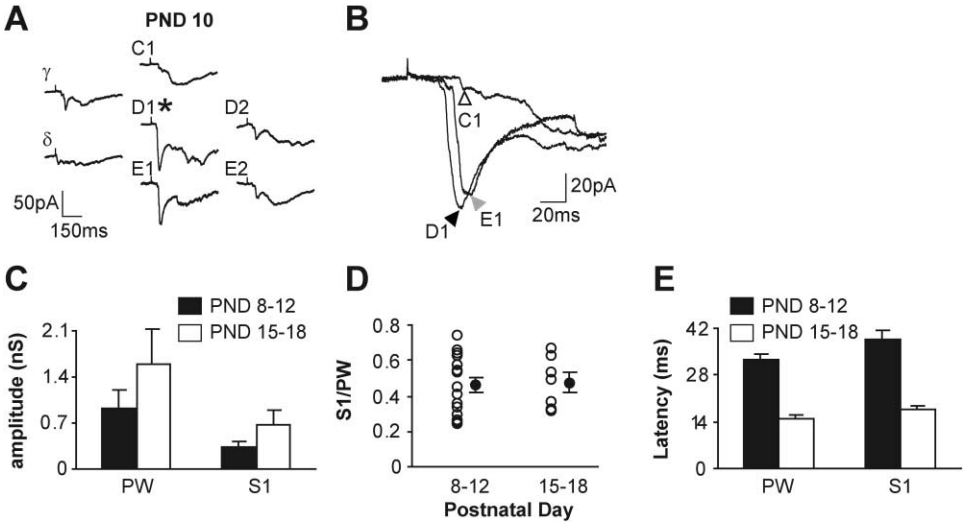

Figure 9. Receptive Fields of Layer 2/3 Cells Have Mature Structure Early during Development

(A) Example of a receptive field (PND 10). Asterisk indicates the principal whisker.

(B) The principal whisker (D1, black arrowhead) produced larger responses with shorter latencies than surround whiskers (E1, gray arrowhead; C1, white arrowhead; same neuron as in A).

(C) Synaptic conductances activated by the principal whisker (PW) and the next-surround whiskers (S1) at PND 8–12 (black) and PND 15–18 (white).

(D) The S1/PW amplitude ratio was the same at PND 8–12 and PND 15–18, indicating that subthreshold receptive fields did not get sharper with development. Individual cells, open circles; average, black circles.

(E) Latencies of responses evoked by the stimulation of PW and S1, at PND 8–12 (black) and PND 15–18 (white).

2002; Moore and Nelson, 1998; Zhu and Connors, 1999). Five out of six neurons recovered histologically were located in the barrel corresponding to the whisker producing the largest response. Despite the changes in seEPSC properties, the structure of receptive fields was similar in both age groups (Figure 9D). Thus, early receptive fields have an essentially mature structure, confirming the existence of an early columnar organization of intracortical connections.

Discussion

We studied the development of cortical circuitry impinging onto layer 2/3 neurons in the rat barrel cortex. LSPS allowed us to map rapidly the development of intracortical synaptic connectivity in brain slices. We found that the synaptic input maps of layer 2/3 neurons develop rapidly over the second postnatal week of life. Development is monotonic and precise, without transient hyperconnectivity at the level of columns. The development of functional inputs from layer 4 is mirrored by the rapid columnar development of layer 4 axons and by the high acuity of early receptive fields.

LSPS for Analysis of Circuit Development

At a single developmental time point, LSPS is a powerful tool for circuit analysis (Callaway and Katz, 1993; Dalva and Katz, 1994; Dantzker and Callaway, 2000; Schubert et al., 2001; Shepherd et al., 2003). In a previous study, we explored the use of "excitation profiles" to quantify the photostimulation of major cell types presynaptic to layer 2/3 pyramidal neurons in barrel cortex at PND 15 (Shepherd et al., 2003). This characterization method involves loose-seal recording to map the spatial distribution of sites of photoexcitability, providing direct estimates of both overall photoexcitability and the spatial resolution of photostimulation.

To quantify the structure of synaptic circuits using LSPS at multiple developmental time points, it is necessary to take into account changes in excitability (Figure 1D). We measured excitation profiles in different layers and at different developmental ages. Layer-wise normalization of input maps can then be achieved by dividing the response amplitudes by the mean number of presynaptic APs. The normalized "synaptic input" maps (Figure 1F) then represents the strength of synaptic connections in space and can be directly compared across different developmental ages.

Monotonic Maturation of Neocortical Columnar Circuits

We studied the development of inputs to layer 2/3 neurons using three approaches. First, we used LSPS to map the spatial distribution of inputs into layer 2/3. The mean horizontal distance of synaptic inputs can be used as a measure of the spatial distribution of presynaptic neurons across barrel rows (Figures 3D and 4D). For both barrel-related and septum-related cells, the mean horizontal distance in layer 2/3 and 4 was constant or increased throughout development. Thus, the most local synaptic connections are made first, followed by more distal connections (Dalva and Katz, 1994).

Second, we used quantitative axon reconstructions to map the spatial distribution of outputs from layer 4 to layer 2/3. Here, similarly, the spread of axonal density in layer 2/3 stayed constant or increased with development. This suggests that refinement by pruning of horizontally overarborized axons is not a mechanism involved in the development of intracortical columnar organization, in agreement with the findings of Bender et al. (2003). However, our results diverge from theirs in that they reported a slight developmental relative sharpening of barrel cell axon distributions. In particular, at PND 8–11 a fraction of layer 4 cells ($\sim$30%) located in barrels projected more axons outside than inside their home column in layer 2/3. Subsequent sharpening of the axonal field occurred by addition of axons preferentially in the home column rather than by a retraction of axons outside (Bender et al., 2003). Differences in methodology (e.g., slice thickness), sampling of layer 4 neurons (e.g., depth of cells within the slice), and analysis criteria (e.g., scoring or excluding cells with truncated axons) may account for the observed differences between the two studies. Our results for axonal distributions (Figures 6 and 7) are at any rate consistent with the lack of change we observed in the horizontal spread of layer 4 inputs received by layer 2/3 cells measured from the synaptic input maps (Figure 3).

Third, we used in vivo whole-cell measurements to study the early development of receptive fields (Figures 8 and 9). The earliest responses (PND 8) were small, consistent with the firing of only a few ($<$10) presynaptic neurons (Figure 8). The developmental maturation of whisker-evoked responses was characterized by shorter latencies, a change in short-term plasticity, and larger response amplitudes. Despite these developmental changes, the structure of receptive fields was similar throughout development and in the mature brain. Layer 2/3 cells migrate into place over a prolonged period (PND 2–6) (Ignacio et al., 1995). We cannot rule out the possibility that during this earliest period different mechanisms of circuit formation, perhaps including transient overarborization, apply.

Our data imply that intracortical circuits develop in a precise, monotonic manner at the level of cortical columns. Anatomical and functional circuits develop almost simultaneously. In addition, columnar organization remains intact even under conditions of sensory deprivation (Bender et al., 2003; Shepherd et al., 2003), suggesting that the establishment of cortical columns is independent of sensory experience (Crowley and Katz, 2002). Instead, the effects of sensory deprivation on receptive fields (Stern et al., 2001) during the critical period are expressed at the level of interlaminar circuits without affecting the horizontal spread of functional columns (Shepherd et al., 2003). Experience-dependent structural plasticity of layer 2/3 dendrites (Maravall et al., 2004a) and spines (Lendvai et al., 2000) likely reflect refinements at the level of these interlaminar circuits.

Developmental Differentiation of Intracortical Circuitry in the Barrel Cortex

The barrel cortex contains distinct circuits related to barrels and septa (Brecht et al., 2003; Brecht and Sakmann, 2002; Kim and Ebner, 1999; Shepherd et al., 2003). In layer 4, this segmentation can easily be seen as early

as the first week (Figure 1A). However, from PND 8 to PND 12, it was difficult to distinguish septum-related and barrel-related synaptic input maps in layer 2/3 (Figure 2). Differences between these circuits developed from PND 12 to PND 16: barrel-related layer 2/3 acquired layer 4 inputs more rapidly than septum-related cells. The timing of this differentiation of layer 2/3 cells into two distinct local-circuit phenotypes coincides with the closure of a critical period for their receptive field development (Stern et al., 2001). Barrel/septum differences were more pronounced in layer 2 than in layer 3, where septum-related neurons had little layer 4 synaptic inputs and pronounced layer 2/3 inputs. Similarly, the distribution of axonal density of barrel and septum cells diverged between PND 12 and 16. Barrel cells continued to grow axons into barrel-related columns, whereas septum cells began to grow axons into neighboring barrel-related columns. These differences may account for the differences in sensory-evoked responses and receptive fields in barrel-related and septum-related layer 2/3 neurons measured in vivo (Brecht et al., 2003).

Mechanisms of Circuit Development

In the canonical model of circuit formation, axons initially project broadly to make diffuse and diverse synaptic circuits (Zigmond et al., 1999). A subset of circuits is stabilized and other circuits are disassembled in an activity-dependent manner. At the level of axons, individual branches are added with little specificity: selection acts at the level of pruning and stabilization (Katz and Shatz, 1996; Ruthazer et al., 2003). For example, retinogeniculate axons from the two eyes project to overlapping regions of the lateral geniculate nucleus (LGN) and later segregate into eye-specific zones (Campbell and Shatz, 1992; Chen and Regehr, 2000; Rakic, 1976; Shatz, 1983). Similar transient states of hyperinnervation are seen in the retinocollicular map (Debski and Cline, 2002; Ruthazer et al., 2003), the neuromuscular junction (Lichtman and Colman, 2000), and the mossy fiber projection in the cerebellum (Crepel et al., 1976). Development of intracortical circuitry could obey different rules. Studies of interlaminar circuitry in the visual cortex have revealed considerable specificity (Borrell and Callaway, 2002; Callaway and Lieber, 1996; Katz, 1991). Laminar targeting may be guided by the precise molecular cues defining laminae (Frantz et al., 1994; Saganich et al., 1999). Such molecular cues have not been described for cortical columns. We find precise and monotonic development of columnar circuitry in the barrel cortex. We note that refinement by synapse elimination may still be an important mechanism underlying the development of intracortical circuitry and receptive fields, but acting within the column (Lendvai et al., 2000; Maravall et al., 2004a; Shepherd et al., 2003; Stern et al., 2001; Takahashi et al., 2003), rather than between columns.

One possible mechanism guiding the precise development of columns could involve chemical gradients. For example, layer 4 axons projecting toward upper layers might be attracted by a diffusible signal; the same signal could repel different axons projecting to lower layers (e.g., Sema 3A; Polleux et al., 2000). Considering the relatively small distance between layer 4 and upper layer 2 ($\sim$500 μm), compared to the distances between the retina and LGN or superior colliculus (millimeters), this alone could be sufficient to generate the precise feedforward circuit contained within a single barrel column. Differences between septum and barrel neurons could arise because of developmental differences in the expression of the relevant receptors or because of activity-dependent competitive mechanisms (Foeller and Feldman, 2004; Katz and Shatz, 1996; Shepherd et al., 2003). A major question is how cortical columns are set up in the first place at the level of layer 4.

Experimental Procedures

Brain Slice Preparation and Electrophysiology

Sprague-Dawley rats (PND 6–16) were used in accordance with institutional guidelines. The three age groups labeled as "PND 8," "PND 12," and "'PND 16" corresponded to the following age ranges (LSPS, axon reconstructions): PND 6–8, PND 11–12, and PND 15–16. Across-whisker-barrel row slices (Finnerty et al., 1999; Shepherd et al., 2003; Welker and Woolsey, 1974) were cut in chilled cutting solution containing (in mM): 110 choline chloride, 25 $NaHCO_3$, 25 D-glucose, 11.6 sodium ascorbate, 7 $MgSO_4$, 3.1 sodium pyruvate, 2.5 KCl, 1.25 NaH_2PO_4, and 0.5 $CaCl_2$. Slices were then transferred to artificial cerebrospinal fluid (ACSF) containing (in mM): 127 NaCl, 25 $NaHCO_3$, 25 D-glucose, 2.5 KCl, 4 $MgCl_2$, 4 $CaCl_2$, and 1.25 NaH_2PO_4, aerated with 95% O_2/5% CO_2. Slices were first incubated at 34°C for $\sim$0.5 hr and then maintained at room temperature prior to use. Slices were 300 μm thick, because this corresponds to the thickness of a barrel and also allows high-quality morphological reconstructions without resectioning. For the above-barrel recording configuration, only slices with at least three contiguous barrels were used, while for the above-septum configuration, two clear barrels were sufficient. Recorded neurons were in barrel rows B–D and β–γ and typically arcs 1–2.

Neurons 40–80 μm deep in the slice were visualized with infrared gradient contrast optics (Dodt et al., 2003) and patched using borosilicate electrodes (5–7 MΩ). Access resistances were in the range 10–35 MΩ. The intracellular solution contained (in mM) 120 Kgluconate, 5 NaCl, 2 $MgCl_2$, 0.1 $CaCl_2$, 10 HEPES, 1.1 EGTA, 4 Mg_2ATP, 0.4 Na_2GTP, 15 sodium phosphocreatine, and 0.015 Alexa-594 (Molecular Probes) (pH 7.25; 290 mOsm). Whole-cell recordings were made using a Multiclamp 700 (Axon Instruments) amplifier. Pyramidal cells were identified by their morphology and firing patterns. Excitatory postsynaptic currents were measured in voltage clamp at $-$70 mV at room temperature. Custom software for instrument control and acquisition was written in Matlab (MathWorks, Inc.).

LSPS by Glutamate Uncaging

LSPS was performed as described in Shepherd et al. (2003). Nitroindolinyl (NI)-caged glutamate (Sigma-RBI; Canepari et al., 2001) was added to recirculating ACSF to a concentration of 0.37 mM. Once whole-cell recording was established, focal photolysis of caged glutamate was accomplished with a 1 ms pulse of a pulsed UV laser (wavelength, 355 nm; repetition rate, 100 kHz; DPSS Lasers, Inc.) consisting of 100 pulses. Laser power was set to a nominal power of 15 mW at the specimen plane. Beam position was controlled with mirror galvanometers (Cambridge Scanning, Inc.). The beam entered the microscope via a dichroic mirror and was focused using an air objective lens (4×, NA 0.1 Olympus). The optics were designed to give a nearly cylindrical beam with a beam diameter of $\sim$15 μm.

The standard stimulus pattern for LSPS mapping consisted of 256 positions on a 16 × 16 grid. Spacing was set to 50 μm between adjacent rows and columns, giving a 750 × 750 μm mapping region. For loose-seal spike recordings, smaller patterns with 64 positions (8 × 8 grid, 350 × 350 μm) were used. To avoid receptor desensitization, glutamate toxicity, and local caged compound depletion, we mapped with a pattern that avoided the vicinity of recently visited sites. During consecutive mapping, we alternated among a set of flipped and rotated variants of this sequence. Individual UV stimuli were presented every 1.5 s. Traces consisted of 100 ms of baseline prior to the stimulus, a 500 ms response interval, and a test pulse for measuring electrophysiological parameters.

Analysis of LSPS Data

Responses (synaptic currents or APs) were analyzed within 100 ms after the UV stimulus. Synaptic responses were automatically parsed into trials containing also direct responses (characterized by rapid onset excitation of postsynaptic receptors) and trials with purely synaptic responses (delay to response $>$ 7 ms). Since trials containing direct responses also contained information about synaptic circuitry, we subtracted direct responses using a template derived from pure (devoid of synaptic currents) direct responses. About half of the traces containing direct responses were corrected. Traces with large direct responses (0.1 to $>$1 nA), which were more prevalent at older ages (PND 12 and 16) and were generally encountered within 50 μm from the soma and along the apical dendrite, were not corrected. Therefore, for horizontal plots of synaptic inputs originating from layer 2/3 (Figure 4), responses were only analyzed in a band across layer 2/3, excluding a vertical band of 100 μm centered in the middle of barrel or septum.

Input maps for individual neurons were constructed by computing the mean current amplitude calculated in a window from 7 to 100 ms after the UV stimulus for each location of photostimulation. Typically 2 to 4 maps were obtained per cell and averaged. These averaged single-cell maps were used to compute group-averaged maps. This was done by aligning brain slices based on images of their barrel architecture. Input maps were then normalized layer-wise to the total number of APs evoked by uncaging in any given layer (Figure 1D). For display only, interpolation was performed on averaged synaptic input maps (Figures 2 and 5). Growth rates of synaptic inputs mentioned in the text were calculated by averaging pixels values in a window with a width of 250 μm and the height of layer 4 or layer 2/3. Mean horizontal distance of synaptic inputs (Figures 3D and 4D) was calculated with the equation Σ(synaptic input $\times$ horizontal distance from barrel or septum center)/Σ(synaptic input).

Reconstructions of Axonal Arbors

In a parallel set of experiments, layer 4 cells located in barrels or septa were recorded with pipettes containing 2 mg/ml of biocytin (in the intracellular solution noted above). Cell bodies were distributed fairly evenly within barrels and septa. Consistent with previous findings, the proportion of pyramidal cells decreased with developmental age in barrels (Bender et al., 2003): our sample consisted of 7 stellate and 11 pyramidal cells at PND 8, 12 stellate and 4 pyramidal cells at PND 12, and 12 stellate and 3 pyramidal cells at PND 16 for neurons in barrels. Most (17/20) septum cells were pyramidal cells (Brecht et al., 2003). Cells were 40–70 μm deep (average 54 μm). After 5–15 min of whole-cell configuration, the pipette was gently pulled out to form an outside-out patch. After allowing for diffusion of the biocytin ($\sim$1 hr), slices were fixed in 4% paraformaldehyde for $\geq$48 hr. Subsequently, slices were rinsed in sodium phosphate buffer, and endogenous peroxidases were quenched with 1% H_2O_2 for 30 min. Slices were processed for avidin-biotin-peroxidase reaction (Vector Laboratories) in tris-buffered solution and mounted in glycerol (Hamam and Kennedy, 2003). By using an aqueous mounting medium and avoiding sample dehydration, tissue shrinkage was minimized, here estimated at $<$1%. Axons arose from a single process emanating from the base of the cell body, did not taper, and had en passant boutons. Dendrites were studded with numerous dendritic spines. The axonal arborization of cells was reconstructed in 3D using a 60$\times$, NA 1.2 objective (Olympus) and Neurolucida software (Microbrightfield). Data were imported into Matlab for further analysis. Axons were analyzed in three dimensions and the data were collapsed into two dimensions to generate a map of the axonal length density (length per (50 μm)^2). For display only, interpolation was performed on group average images (Figures 6B and 6C). Mean horizontal distance of axons (Figure 7G) was calculated with the equation Σ(axonal length density $\times$ horizontal distance from soma)/Σ(axonal length density).

In Vivo Electrophysiology

Rats (PND 8–18) were anesthetized (urethane i.p. 1.5–1.75 mg/kg) and placed in a stereotaxic apparatus. To monitor the depth of anesthesia, an EEG electrode was inserted between the skull and the dura, posterior to the barrel cortex. If necessary, anesthesia was supplemented with urethane (10% of the original dose). A 3 $\times$ 3 mm craniotomy was made above barrel cortex and the dura was opened.

Patch electrodes (5.5–6 MΩ) were filled with internal solution containing (in mM): 120 $CsMeSO_3$, 5 NaCl, 10 HEPES, 1.1 EGTA, 2 $MgCl_2$, 0.1 $CaCl_2$, 5 QX-314, 4 Mg-ATP, 0.4 Na-GTP, and 2 mg/ml biocytin (290 mOsm, pH 7.4). Blind whole-cell recordings were made using an Axopatch-200B (Axon Instruments) amplifier. Electrode capacitance was compensated. Cells had an input resistance (R_{in}) of 251 $\pm$ 32 MΩ. Series resistance (R_s) (83 $\pm$ 6 MΩ) was not compensated, but membrane potential was corrected offline for R_s using the relationship $Vm' = V_{command} - R_s \times I$ (I = amplitude of seEPSC) (Borg-Graham et al., 1998). There was no correlation between seEPSC amplitudes and R_s, R_{in}, or the ratio R_{in}/R_s. Electrodes for local field potential recording were filled with NaCl 1 M. Single whiskers on the contralateral side were stimulated using a glass pipette mounted on a piezoelectric wafer. For each stimulus trial, a whisker was moved up and, after 1 s, down. The movement was $\sim$0.5 mm at $\sim$1 mm away from the skin. 5–15 trials were collected every 13 s for whole-cell recording and every 3 or 15 s for local field potential recording.

Rise- (20%–80%) and half-decay times were measured on selected isolated spontaneous synaptic currents (sPSCs) at $-$70 mV (15 neurons; 398 sPSCs). sPSC amplitudes ranged from 5 to 120 pA.

Whisker-evoked responses to the upward stimulus were analyzed. Each stimulus evoked a barrage of responses. In PND 8–12 rats, individual trials were inspected to set the limits within which the peak amplitude would be detected in order to minimize the contribution of later events (Figure 8D). On average, the amplitudes of early responses were measured at 9.7 $\pm$ 3.5 ms after the onset at PND 8–12 and at 8 ms after the onset in PND 15–18 rats. The average seEPSC was computed and used to calculate the conductances (g) according to the equation $g = I/Vm'$.

Receptive fields were measured by stimulating whiskers in a pseudorandom order. Acuity of receptive field was assessed by averaging the conductances activated by the first (S1) order of surrounding whiskers located in the same rank or row (diagonals were excluded) and expressed this measurement as a ratio of the conductance activated by the principal whisker (Stern et al., 2001).

After completion of electrophysiological experiments, rats were perfused transcardially with cold saline solution and 4% paraformaldehyde in sodium phosphate buffer. The brain was removed and flattened to allow tangential sectioning. The brain was sectioned (100 μm) and processed for biocytin and counterstained for cytochrome oxidase. Each neuron was assigned to a principal whisker by aligning the section containing the soma or basal dendrites with the sections containing the barrels in layer 4.

Error bars are given as standard errors of the mean (SEM) unless stated otherwise.

Acknowledgments

We thank T.A. Pologruto and T. O'Connor for help with programming, B.A. Burbach and S.M. Sternson for technical input, C. Wu and Z.J. Huang for Neurolucida support, and E. Ruthazer for comments on the manuscript. Support by HFSP and Fyssen (I.B.), HHMI (G.M.G.S., K.S.), and NIH (K.S.).

Received: January 28, 2004
Revised: March 23, 2004
Accepted: April 22, 2004
Published: June 9, 2004

References

Agmon, A., and Connors, B.W. (1991). Thalamocortical responses of mouse somatosensory (barrel) cortex in vitro. Neuroscience *41*, 365–379.

Agmon, A., Yang, L.T., O'Dowd, D.K., and Jones, E.G. (1993). Organized growth of thalamocortical axons from the deep tier of terminations into layer IV of developing mouse barrel cortex. J. Neurosci. *13*, 5365–5382.

Albus, K., and Wolf, W. (1984). Early post-natal development of neuronal function in the kitten's visual cortex: a laminar analysis. J. Physiol. *348*, 153–185.

Armstrong-James, M. (1975). The functional status and columnar organization of single cells responding to cutaneous stimulation in neonatal rat somatosensory cortex S1. J. Physiol. *246*, 501–538.

Armstrong-James, M., and Fox, K. (1987). Spatiotemporal convergence and divergence in the rat S1 "barrel" cortex. J. Comp. Neurol. *263*, 265–281.

Bender, K.J., Rangel, J., and Feldman, D.E. (2003). Development of columnar topography in the excitatory layer 4 to layer 2/3 projection in rat barrel cortex. J. Neurosci. *23*, 8759–8770.

Bernardo, K.L., and Woolsey, T.A. (1987). Axonal trajectories between mouse somatosensory thalamus and cortex. J. Comp. Neurol. *258*, 542–564.

Borg-Graham, L.J., Monier, C., and Fregnac, Y. (1998). Visual input evokes transient and strong shunting inhibition in visual cortical neurons. Nature *393*, 369–373.

Borrell, V., and Callaway, E.M. (2002). Reorganization of exuberant axonal arbors contributes to the development of laminar specificity in ferret visual cortex. J. Neurosci. *22*, 6682–6695.

Brecht, M., and Sakmann, B. (2002). Dynamic representation of whisker deflection by synaptic potentials in spiny stellate and pyramidal cells in the barrels and septa of layer 4 rat somatosensory cortex. J. Physiol. *543*, 49–70.

Brecht, M., Roth, A., and Sakmann, B. (2003). Dynamic receptive fields of reconstructed pyramidal cells in layers 3 and 2 of rat somatosensory barrel cortex. J. Physiol. *553*, 243–265.

Brennan, E.M., Martin, L.J., Johnston, M.V., and Blue, M.E. (1997). Ontogeny of non-NMDA glutamate receptors in rat barrel field cortex. II. Alpha-AMPA and kainate receptors. J. Comp. Neurol. *386*, 29–45.

Brown, A., Yates, P.A., Burrola, P., Ortuno, D., Vaidya, A., Jessell, T.M., Pfaff, S.L., O'Leary, D.D., and Lemke, G. (2000). Topographic mapping from the retina to the midbrain is controlled by relative but not absolute levels of EphA receptor signaling. Cell *102*, 77–88.

Callaway, E.M., and Katz, L.C. (1990). Emergence and refinement of clustered horizontal connections in cat striate cortex. J. Neurosci. *10*, 1134–1153.

Callaway, E.M., and Katz, L.C. (1993). Photostimulation using caged glutamate reveals functional circuitry in living brain slices. Proc. Natl. Acad. Sci. USA *90*, 7661–7665.

Callaway, E.M., and Lieber, J.L. (1996). Development of axonal arbors of layer 6 pyramidal neurons in ferret primary visual cortex. J. Comp. Neurol. *376*, 295–305.

Campbell, G., and Shatz, C.J. (1992). Synapses formed by identified retinogeniculate axons during the segregation of eye input. J. Neurosci. *12*, 1847–1858.

Canepari, M., Nelson, L., Papageorgiou, G., Corrie, J.E., and Ogden, D. (2001). Photochemical and pharmacological evaluation of 7-nitroindolinyl-, and 4-methoxy-7-nitroindolinyl-amino acids as novel, fast caged neurotransmitters. J. Neurosci. Methods *112*, 29–42.

Chen, C., and Regehr, W.G. (2000). Developmental remodeling of the retinogeniculate synapse. Neuron *28*, 955–966.

Chmielowska, J., Carvell, G.E., and Simons, D.J. (1989). Spatial organization of thalamocortical and corticothalamic projection systems in the rat SmI barrel cortex. J. Comp. Neurol. *285*, 325–338.

Crepel, F., Mariani, J., and Delhaye-Bouchaud, N. (1976). Evidence for a multiple innervation of Purkinje cells by climbing fibers in the immature rat cerebellum. J. Neurobiol. *7*, 567–578.

Crowley, J.C., and Katz, L.C. (2002). Ocular dominance development revisited. Curr. Opin. Neurobiol. *12*, 104–109.

Dalva, M.B., and Katz, L.C. (1994). Rearrangements of synaptic connections in visual cortex revealed by laser photostimulation. Science *265*, 255–258.

Dantzker, J.L., and Callaway, E.M. (2000). Laminar sources of synaptic input to cortical inhibitory interneurons and pyramidal neurons. Nat. Neurosci. *3*, 701–707.

Debski, E.A., and Cline, H.T. (2002). Activity-dependent mapping in the retinotectal projection. Curr. Opin. Neurobiol. *12*, 93–99.

Dodt, H.U., Eder, M., Schierloh, A., and Zieglgansberger, W. (2003). Infrared-guided laser stimulation of neurons in brain slices. Science's STKE, e35.

Finnerty, G.T., Roberts, L.S., and Connors, B.W. (1999). Sensory experience modifies the short-term dynamics of neocortical synapses. Nature *400*, 367–371.

Foeller, E., and Feldman, D.E. (2004). Synaptic basis for developmental plasticity in somatosensory cortex. Curr. Opin. Neurobiol. *14*, 89–95.

Fox, K. (1992). A critical period for experience-dependent synaptic plasticity in rat barrel cortex. J. Neurosci. *12*, 1826–1838.

Frantz, G.D., Weimann, J.M., Levin, M.E., and McConnell, S.K. (1994). Otx1 and Otx2 define layers and regions in developing cerebral cortex and cerebellum. J. Neurosci. *14*, 5725–5740.

Fregnac, Y., and Imbert, M. (1978). Early development of visual cortical cells in normal and dark-reared kittens: relationship between orientation selectivity and ocular dominance. J. Physiol. *278*, 27–44.

Hamam, B.N., and Kennedy, T.E. (2003). Visualization of the dendritic arbor of neurons in intact 500 microm thick brain slices. J. Neurosci. Methods *123*, 61–67.

Hubel, D.H., and Wiesel, T.N. (1962). Receptive fields, binocular interaction and functional architecture in the cat's visual cortex. J. Physiol. (London) *148*, 574–591.

Hubel, D.H., and Wiesel, T.N. (1963). Receptive fields of cells in striate cortex of very young, visually inexperienced kittens. J Neurophysiol *26*, 994–1002.

Ignacio, M.P., Kimm, E.J., Kageyama, G.H., Yu, J., and Robertson, R.T. (1995). Postnatal migration of neurons and formation of laminae in rat cerebral cortex. Anat. Embryol. (Berl.) *191*, 89–100.

Jhaveri, S., Erzurumlu, R.S., and Crossin, K. (1991). Barrel construction in rodent neocortex: role of thalamic afferents versus extracellular matrix molecules. Proc. Natl. Acad. Sci. USA *88*, 4489–4493.

Katz, L.C. (1991). Specificity in the development of vertical connections in cat striate cortex. Eur. J. Neurosci. *3*, 1–9.

Katz, L.C., and Shatz, C.J. (1996). Synaptic activity and the construction of cortical circuits. Science *274*, 1133–1138.

Kidd, F.L., Coumis, U., Collingridge, G.L., Crabtree, J.W., and Isaac, J.T. (2002). A presynaptic kainate receptor is involved in regulating the dynamic properties of thalamocortical synapses during development. Neuron *34*, 635–646.

Killackey, H.P., and Leshin, S. (1975). The organization of specific thalamocortical projections to the posteromedial barrel subfield of the rat somatic sensory cortex. Brain Res. *86*, 469–472.

Killackey, H.P., Rhoades, R.W., and Bennett-Clarke, C.A. (1995). The formation of a cortical somatotopic map. Trends Neurosci. *18*, 402–407.

Kim, U., and Ebner, F.F. (1999). Barrels and septa: separate circuits in rat barrels field cortex. J. Comp. Neurol. *408*, 489–505.

Koralek, K.A., Jensen, K.F., and Killackey, H.P. (1988). Evidence for two complementary patterns of thalamic input to the rat somatosensory cortex. Brain Res. *463*, 346–351.

Leinekugel, X., Khazipov, R., Cannon, R., Hirase, H., Ben-Ari, Y., and Buzsaki, G. (2002). Correlated bursts of activity in the neonatal hippocampus in vivo. Science *296*, 2049–2052.

Lendvai, B., Stern, E., Chen, B., and Svoboda, K. (2000). Experience-dependent plasticity of dendritic spines in the developing rat barrel cortex *in vivo*. Nature *404*, 876–881.

Lev, D.L., Weinfeld, E., and White, E.L. (2002). Synaptic patterns of thalamocortical afferents in mouse barrels at postnatal day 11. J. Comp. Neurol. *442*, 63–77.

Lichtman, J.W., and Colman, H. (2000). Synapse elimination and indelible memory. Neuron *25*, 269–278.

Lin, D.M., Wang, F., Lowe, G., Gold, G.H., Axel, R., Ngai, J., and Brunet, L. (2000). Formation of precise connections in the olfactory bulb occurs in the absence of odorant-evoked neuronal activity. Neuron *26*, 69–80.

Lu, S.M., and Lin, R.C.S. (1992). Thalamic afferents of the rat barrel cortex: a light- and electron-microscopic study using *Phaseolus*

vulgaris leucoagglutinin as an anterograde tracer. Somatosens. Mot. Res. *10*, 1–16.

Lubke, J., Roth, A., Feldmeyer, D., and Sakmann, B. (2003). Morphometric analysis of the columnar innervation domain of neurons connecting layer 4 and layer 2/3 of juvenile rat barrel cortex. Cereb. Cortex *13*, 1051–1063.

Maravall, M., Koh, I.Y.Y., Lindquist, W.B., and Svoboda, K. (2004a). Experience-dependent changes in basal dendritic branching of layer 2/3 pyramidal neurons during a critical period for developmental plasticity in rat barrel cortex. Cereb. Cortex, in press. Published online March 28, 2004. 10.1093/cercor/bhh026

Maravall, M., Stern, E.A., and Svoboda, K. (2004b). Development of intrinsic properties and excitability of layer 2/3 pyramidal neurons during a critical period for sensory maps in rat barrel cortex. J. Neurophysiol., in press. Published online February 18, 2004. 10.1152/jn.00598.2003

Micheva, K.D., and Beaulieu, C. (1996). Quantitative aspects of synaptogenesis in the rat barrel field cortex with special reference to GABA circuitry. J. Comp. Neurol. *373*, 340–354.

Moore, C.I., and Nelson, S.B. (1998). Spatio-temporal subthreshold receptive fields in the vibrissa representation of rat primary somatosensory cortex. J. Neurophysiol. *80*, 2882–2892.

Mountcastle, V.B. (1957). Modality and topographic properties of single neurons of cat's somatic sensory cortex. J. Neurophysiol. *20*, 408–434.

Petersen, C.C., and Sakmann, B. (2001). Functionally independent columns of rat somatosensory barrel cortex revealed with voltage-sensitive dye imaging. J. Neurosci. *21*, 8435–8446.

Polleux, F., Morrow, T., and Ghosh, A. (2000). Semaphorin 3A is a chemoattractant for cortical apical dendrites. Nature *404*, 567–573.

Rakic, P. (1976). Prenatal genesis of connections subserving ocular dominance in the rhesus monkey. Nature *261*, 467–471.

Rice, F.L., and Van der Loos, H. (1977). Development of the barrels and barrel field in the somatosensory cortex of the mouse. J. Comp. Neurol. *171*, 545–560.

Roerig, B., and Kao, J.P. (1999). Organization of intracortical circuits in relation to direction preference maps in ferret visual cortex. J. Neurosci. *19*, RC44.

Ruthazer, E.S., Akerman, C.J., and Cline, H.T. (2003). Control of axon branch dynamics by correlated activity in vivo. Science *301*, 66–70.

Saganich, M.J., Vega-Saenz de Miera, E., Nadal, M.S., Baker, H., Coetzee, W.A., and Rudy, B. (1999). Cloning of components of a novel subthreshold-activating K(+) channel with a unique pattern of expression in the cerebral cortex. J. Neurosci. *19*, 10789–10802.

Schlaggar, B.L., and O'Leary, D.D. (1994). Early development of the somatotopic map and barrel patterning in rat somatosensory cortex. J. Comp. Neurol. *346*, 80–96.

Schlaggar, B.L., Fox, K., and O'Leary, D.D.M. (1993). Postsynaptic control of plasticity in developing somatosensory cortex. Nature *364*, 623–626.

Schubert, D., Staiger, J.F., Cho, N., Kotter, R., Zilles, K., and Luhmann, H.J. (2001). Layer-specific intracolumnar and transcolumnar functional connectivity of layer V pyramidal cells in rat barrel cortex. J. Neurosci. *21*, 3580–3592.

Shatz, C.J. (1983). The prenatal development of the cat's retinogeniculate pathway. J. Neurosci. *3*, 482–499.

Shepherd, G.M., Pologruto, T.A., and Svoboda, K. (2003). Circuit analysis of experience-dependent plasticity in the developing rat barrel cortex. Neuron *38*, 277–289.

Simons, D.J. (1978). Response properties of vibrissa units in rat SI somatosensory neocortex. J. Neurophysiol. *41*, 798–820.

Stern, E.A., Maravall, M., and Svoboda, K. (2001). Rapid development and plasticity of layer 2/3 maps in rat barrel cortex in vivo. Neuron *31*, 305–315.

Takahashi, T., Svoboda, K., and Malinow, R. (2003). Experience strengthening transmission by driving AMPA receptors into synapses. Science *299*, 1585–1588.

Ullensvang, K., Lehre, K.P., Storm-Mathisen, J., and Danbolt, N.C. (1997). Differential developmental expression of the two rat brain glutamate transporter proteins GLAST and GLT. Eur. J. Neurosci. *9*, 1646–1655.

Van der Loos, H., and Woolsey, T.A. (1973). Somatosensory cortex: structural alterations following early injury to sense organs. Science *179*, 395–398.

Waite, P.M., and Taylor, P.K. (1978). Removal of whiskers in young rats causes functional changes in cerebral cortex. Nature *274*, 600–602.

Welker, C., and Woolsey, T.A. (1974). Structure of layer IV in the somatosensory neocortex of the rat: description and comparison with the mouse. J. Comp. Neurol. *158*, 437–453.

White, E.L., and DeAmicis, R.A. (1977). Afferent and efferent projections of the region in mouse SmL cortex which contains the posteromedial barrel subfield. J. Comp. Neurol. *175*, 455–482.

Woolsey, T.A., and Van der Loos, H. (1970). The structural organization of layer IV in the somatosensory region (S1) of mouse cerebral cortex. Brain Res. *17*, 205–242.

Zheng, C., Feinstein, P., Bozza, T., Rodriguez, I., and Mombaerts, P. (2000). Peripheral olfactory projections are differentially affected in mice deficient in a cyclic nucleotide-gated channel subunit. Neuron *26*, 81–91.

Zhu, J.J. (2000). Maturation of layer 5 neocortical pyramidal neurons: amplifying salient layer 1 and layer 4 inputs by Ca^{2+} action potentials in adult rat tuft dendrites. J. Physiol. *526*, 571–587.

Zhu, J.J., and Connors, B.W. (1999). Intrinsic firing patterns and whisker-evoked synaptic responses of neurons in the rat barrel cortex. J. Neurophysiol. *81*, 1171–1183.

Zigmond, M.J., Bloom, F.E., Landis, S.C., Roberts, J.L., and Squire, L.R. (1999). Fundamental Neuroscience, First edition (New York: Academic Press).